Article

Not peer-reviewed version

Detailed Investigation on Ambiguity Validation of Long-Distance RTK

Shengyue Ji , Jing Wang , Duojie Weng * , Wu Chen

Posted Date: 2 July 2024

doi: 10.20944/preprints202407.0220.v1

Keywords: long-distance RTK; ambiguity resolution; ambiguity validation; success rate; R-ratio test

Article

Detailed Investigation on Ambiguity Validation of Long-Distance RTK

Shengyue Ji [1], Jing Wang [1], Duojie Weng [2]* and Wu Chen [2]

[1] China University of Petroleum (East China), Qingdao, China
[2] The Hong Kong Polytechnic University, Hong Kong, China
* Correspondence: author email: wengduojie.lsgi@polyu.edu.hk

Abstract: Long-distance Real-Time Kinematic (RTK) positioning is crucial for applications in remote areas, such as maritime environments. Achieving 2-3 cm accuracy with RTK requires successful ambiguity resolution, which involves two main two steps: identifying the best integer ambiguity candidate and confirming its validity. While previous research has largely concentrated on the first step, including the development of Cascading Ambiguity Resolution methods, and reducing tropospheric delay, studies on the validation of ambiguity for long-distance RTK are limited. This study conducts a thorough examination of ambiguity validation for long-distance RTK, focusing on two prevalent methods: the theoretical success rate and the R-ratio test. The results reveal several key insights. Firstly, the six commonly used bounds for the theoretical success rate are not accurate reflection of the actual success rate, making them unsuitable for long-distance RTK applications. Secondly, the R-ratio test proves to be dependable when the threshold is set above 1.7, assuming there is a minimum observation period of one minute and at least ten satellites are visible. However, the probability of successfully resolving ambiguities with the R-ratio test does not surpass 50%. Additionally, if ambiguity resolution is not achieved within 20 minutes, simply prolonging the observation time is generally unproductive. To improve the performance of ambiguity resolution in practical situations that require extended observation times, this research proposes a novel ambiguity validation method. This new approach is based the duration for which an integer ambiguity resolution candidate maintaining the best status. This method aims to provide a reliable means of validating ambiguities in case that the R-ratio test fails.

Keywords: long-distance RTK; ambiguity resolution; ambiguity validation; success rate; R-ratio test

1. Introduction

Real-time Kinematic Positioning (RTK) stands as the pinnacle of precision in navigation and positioning technologies, boasting accuracies within 2-3 cm range. Its widespread application across various fields underscores its significance. The successful deployment of RTK hinges on accurately determining the initial integer ambiguity parameters. This task is straightforward and reliable for short to medium distances (Network RTK), yet it becomes considerably more complex for long-distance scenarios. Consequently, RTK technology has been mature application in densely populated regions where setting up nearby reference stations is feasible. However, its application in remote or oceanic areas remains underdeveloped due to the extensive distances between reference stations and users, often exceeding 100 km.

This study primarily addresses long-distance RTK in the context of single-baseline scenarios, which are sometimes the only viable option for specific areas, such as oceans. Unlike network RTK, certain positioning errors, including ionospheric and tropospheric delays, cannot be mitigated and must be estimated. This requirement complicates the observation equations, making them more susceptible to noise and multipath effects, thereby complicating ambiguity resolution.

Historically, research on single-baseline long-distance RTK has concentrated on methods for ambiguity resolution, such as Cascading Ambiguity Resolution (CAR) (Li et al., 2010a; Li et al., 2014; Chu et al., 2016) and partial ambiguity resolution (Li et al., 2014; Li et al., 2018), alongside

 doi:10.20944/preprints202407.0220.v1

investigations into the effects of tropospheric errors (Li et al., 2010b; Shu et al., 2015; Xu et al., 2015) and the performance of various GNSS-system combinations (Chu and Yang, 2013; Odolinski et al., 2015;Zhang et al., 2020a; Zhang et al., 2020b; Sermet et al., 2023). Ambiguity validation, for long baselines, has received less attention, though sometimes discussed theoretically without practical testing (Odijk et al., 2014).

This research shifts focus towards ambiguity validation, exploring two widely recognized methods: the theoretical success rate (Teunissen, 1998a; Teunissen 1998b) and the empirical R-ratio test (Euler and Schaffrin 1991; Leick 2004; Teunissen and Verhagen 2009). While the theoretical success rate evaluates the robustness of mathematical equations based on satellite geometry and data quality, the R-ratio test assess the superiority of the best ambiguity resolution candidate. Although effective for short baselines and potentially in combination, these methods face challenges in long-distance RTK applications.

Through extensive practical experimentation across baselines ranging from 100 km to 300 km within the IGS network, this study scrutinizes the applicability of these ambiguity validation methods. Findings indicate that traditional theoretical success rate methods falter in long-distance RTK contexts, offering bounds too imprecise for practical use. Conversely, the R-ratio test, with a threshold value of 2.0 or lower, proves reliable under sufficient observation durations and satellite visibility. However, only about a third of the experimental cases can be fixed with a threshold value of 2.0 and no more than 50% even with 1.3. And if failing to reach the threshold value in 20 minutes, it is generally useless by extending observation time. The findings highlight the need for a new approach for practical applications.

To address these challenges, this paper proposes a novel ambiguity validation method tailored for extended observation periods. The document is organized as follows: an introduction to the experimental setup, a discussion on the efficacy of existing validation methods, the introduction of the new method, and concluding remarks.

2. Mathematical Model of Long-Distance RTK

The mathematical model of long-distance RTK is generally as follows:

$$AX + BN + MZ + CI = L \quad (1)$$

where X is user coordinates; N is ambiguity vector; Z is zenith tropospheric error; I is ionospheric error; A, B, M and C are corresponding coefficients; L is double-differenced code and carrier phase observation vector. The variance-covariance matrix Q is established based on elevation-dependent weighting scheme with standard deviations of 0.3 m and 0.003 m for code and carrier phase observation noises, respectively.

The process of solving Eq. (1) is as follows. First, get the float ambiguity resolution $\hat{N}$ with Kalman filtering, then search and validate the best integer ambiguity resolution $\breve{N}$ with $(\hat{N} - \breve{N})^T Q_{\hat{N}\hat{N}}^{-1} (\hat{N} - \breve{N}) = min$ ($Q_{\hat{N}\hat{N}}$ denoted as the variance-covariance matrix of $\hat{N}$), finally, estimate X with the fixed ambiguity resolution.

R-ratio test is generally used for ambiguity validation with:

$$R = \frac{(\hat{N} - \breve{N}_{second})^T Q_{\hat{N}\hat{N}}^{-1} (\hat{N} - \breve{N}_{second})}{(\hat{N} - \breve{N}_{best})^T Q_{\hat{N}\hat{N}}^{-1} (\hat{N} - \breve{N}_{best})} \quad (2)$$

where $\breve{N}_{best}$ and $\breve{N}_{second}$ are the best and second-best integer ambiguity resolution.

3. Experimental Design

The GNSS data utilized for this study were sourced exclusively from the International GNSS Service (IGS) network. Initially, baselines were established between various pairs of IGS stations. Subsequently, the focus narrowed to those spanning distances from 100 km to 300 km, resulting in a selection of 80 distinct baselines. For each baseline, four separate one-hour observational sessions were analyzed, specially at 00:00, 06:00, 12:00, and 18:00 on January 1, 2023. This culminated in approximately 320 experimental cases, which were processed in both static and kinematic modes. The primary data processing configurations are summarized in Table 1.

 doi:10.20944/preprints202407.0220.v1

Table 1. Main settings of data processing.

Type	Processing strategy
Code noise standard deviation	0.3m
Phase noise standard deviation	0.003m
Weighting scheme	Elevation dependent
Frequency	Dual and multiple
Positioning mode	Static and kinematic
Data interval	1s
Ionosphere correction	Estimate TEC
Elevation mask	15°
Satellite ephemeris/clock	Real-time precise Ephemeris
Tropospheric dry delay	Model correction
Tropospheric wet delay	Estimate ZTD
Receiver antenna phase center bias	IGS_14.atx
Parameter estimation method	Kalman filtering
Solid earth tide correction	Model correction
Relative correction	Model correction
Wind-up correction	Model correction
Ambiguity resolution	Float and integer
Outlier detection and rejection	Yes
Satellites with single frequency observation	Excluded

The static processing results serve as a benchmark to validate the kinematic ambiguity resolution outcomes. To maximize the credibility of the static ambiguity resolution, two criteria were established. Firstly, the static positioning coordinates must align with the IGS weekly final station solutions (SNX file), with discrepancies not exceeding 1 cm in the horizontal directions and 3 cm in the vertical direction. Secondly, the duration for which a solution is the best ambiguity resolution candidate must exceed thirty minutes, whether consecutively or in intervals. In the latter case, the total duration is calculated by summing all individual segments. Figure 2 illustrates the positioning errors for the best ambiguity resolution (in blue) and the float solution (in red) for experimental case No. 125. The two periods marked by arrows represent the intervals of one ambiguity resolution, and their combined length constitutes the total duration of this resolution. Cases that fail to meet these criteria are excluded from the study. After applying these filters, 307 experimental cases remained and were sequentially numbered. Detailed information on the experimental cases can be found in Appendix A. The global distribution of the cases is shown in Figure 2.

 doi:10.20944/preprints202407.0220.v1

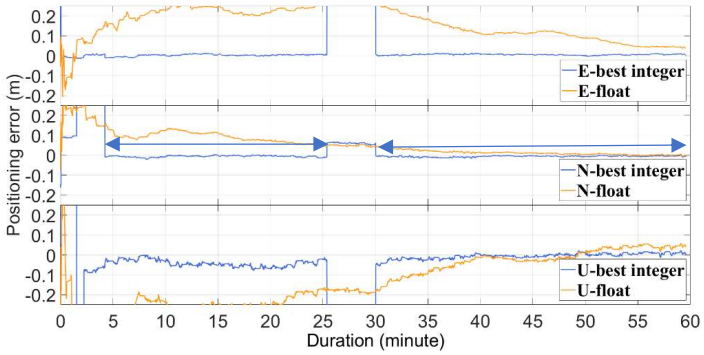

Figure 1. Positioning errors of experimental case No. 125.

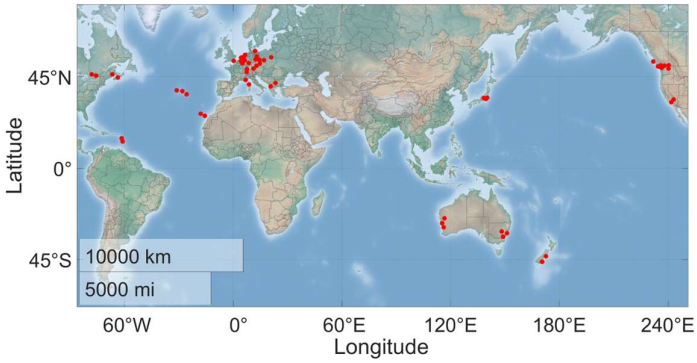

Figure 2. Global distribution of the experimental baselines.

4. Numerical Results

In this section, we present a detailed examination of the experimental outcomes. Initially, we provide a synopsis of the performance in resolving ambiguities, followed by an assessment of the performance in validating ambiguities, which includes an analysis of the theoretical success rate and the R-ratio test.

4.1. Overview of the Experimental Results

The objective of this subsection is to give an overview of ambiguity resolution performance, including the minimum time required to fix ambiguity, the R-ratio performance in one minute and one hour, and a comparison of convergence time and positioning accuracy between the best and float ambiguity resolution.

4.1.1. Minimum Required Time to Fix Ambiguity

Here, we explore the earliest time of the best integer ambiguity resolutions being able to be determined to be correct and subsequently remains constant as shown in Figure 3 or stable in spite of interruption as shown in Figure 1. Theoretically, it should represent the minimum time necessary to resolve ambiguities, irrespective of the ambiguity validation method employed.

 doi:10.20944/preprints202407.0220.v1

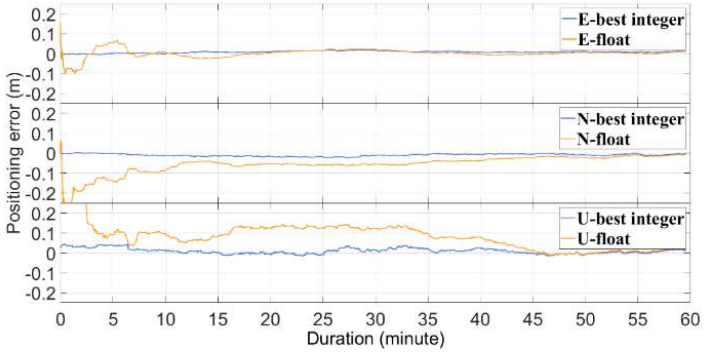

Figure 3. Positioning errors of experimental case No. 38 (dual frequency).

Figure 4 displays the minimum time necessary to correctly resolve ambiguities, with the left side pertaining to dual-frequency scenarios and the right side to multi-frequency scenarios. Figure 5 provides statistical analysis of these times. It is evident that in both scenarios, there are instances where ambiguities can be correctly fixed in a single epoch; approximately 10% of such cases occur in dual-frequency scenarios, while the figure exceeds 20% for multi-frequency scenarios. For the remaining experimental cases, the minimum time required to resolve ambiguities typically ranges from one minute to thirty minutes. Additionally, in both scenarios, there are instances where ambiguities cannot be resolved correctly even after one hour.

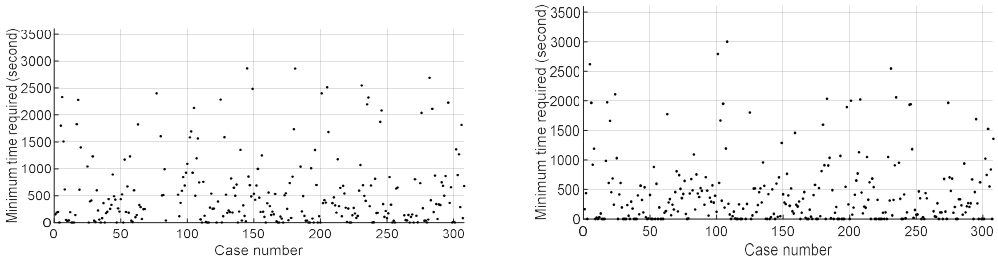

Figure 4. Minimum required time to fix ambiguity (left: dual frequency; right: multiple frequency).

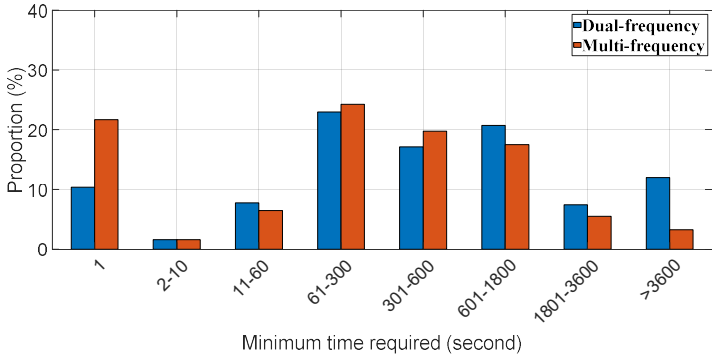

Figure 5. Statistics of the minimum required time to fix ambiguity.

4.1.2. Maximum R-Ratio in One Minute and One Hour

Figures 6 and 7 present the maximum R-ratio values attained within one minute and one hour, respectively, for both dual- and multi-frequency scenarios. Black dots represent instances of correct ambiguity resolution, whereas red dots denote incorrect resolutions. Figure 8 compiles statistics of the peak R-ratio values observed.

Preprints.org (www.preprints.org) | NOT PEER-REVIEWED | Posted: 2 July 2024 doi:10.20944/preprints202407.0220.v1

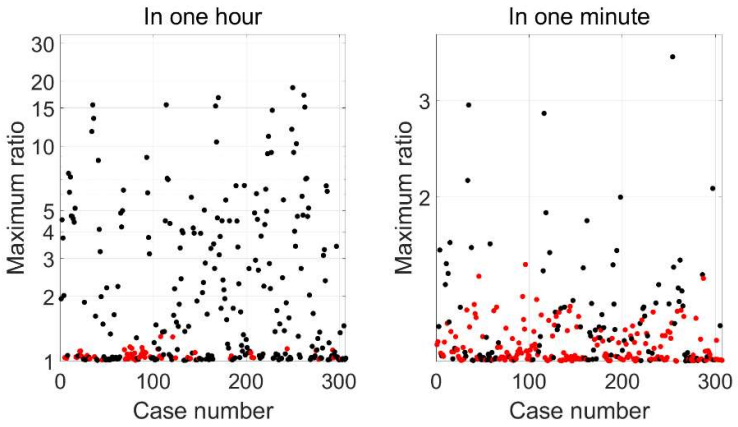

Figure 6. Maximum R-ratio in one hour and one minute (dual-frequency).

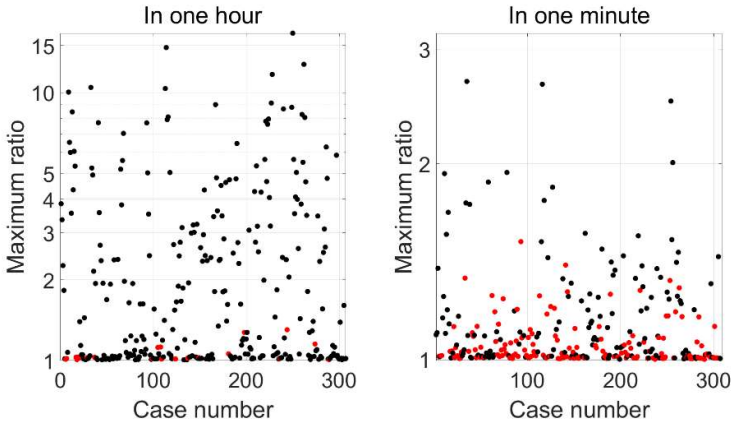

Figure 7. Maximum R-ratio in one hour and one minute (multi-frequency).

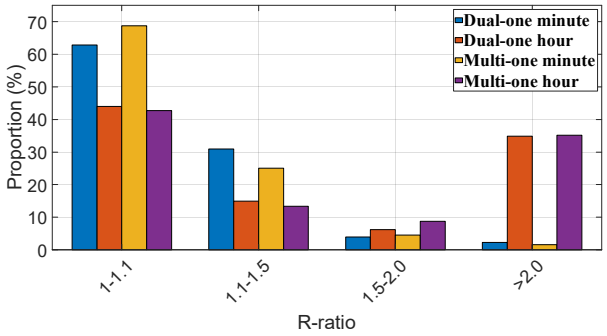

Figure 8. Statistics of the maximum R-ratio.

From the data, it is apparent that in both dual- and multi-frequency scenarios, the majority of the maximum R-ratio values cluster between 1.0 and 1.1, regardless of whether the duration is one minute or one hour. Approximately 35% of the experimental cases exhibit an R-ratio greater than 2.0 after an hour, in contrast to only about 2% reaching the level within one minute.

4.1.3. Convergence Time

Convergence time to reach centimeter-level accuracy is usually used as a measure to assess the performance with float ambiguity resolution in both PPP and long-distance RTK. In this section, the

Preprints.org (www.preprints.org) | NOT PEER-REVIEWED | Posted: 2 July 2024 doi:10.20944/preprints202407.0220.v1

convergence time is also investigated with the best integer ambiguity resolution no matter it is correct or not and compared to that of the float ambiguity resolution.

Figure 9 depicts the time required for positioning errors in both the north and east directions to fall below 10 cm. The blue bar represents the best integer ambiguity resolution. It is observed that, in the dual-frequency scenario illustrated on the left, over 10% of the experimental cases achieve centimeter-level accuracy in a single epoch, whereas in the multi-frequency scenario on the right, this figure rises to about 25%. However, for the remaining cases, reaching such accuracy typically requires between one minute and thirty minutes. The red bar indicates the float ambiguity resolution. In both dual- and multi-frequency scenarios, less than 1% of cases achieve the desired accuracy in a single epoch, with the necessary time predominantly ranging from 10 minutes to thirty minutes.

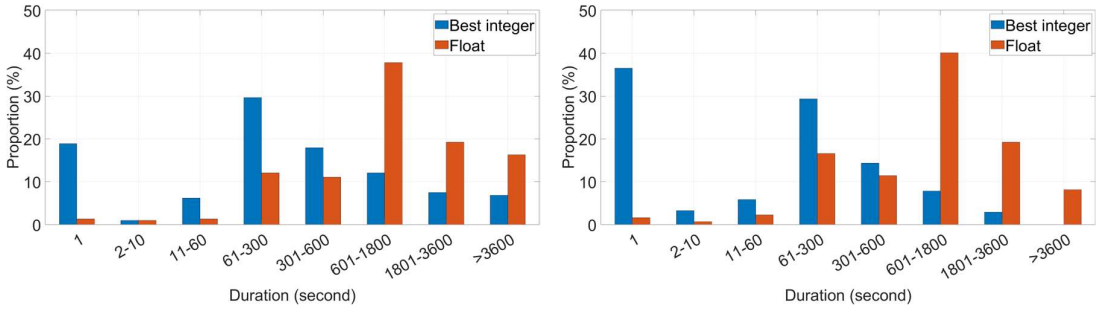

Figure 9. Convergence time with the best integer and float ambiguity resolution in horizontal directions (left: dual frequency; right: multiple frequency).

Figure 10 shows the convergence time in the vertical direction, with results mirroring those in the horizontal directions. Thus, in terms of convergence time, the best integer ambiguity resolution, regardless of its correctness, outperforms the float solution. However, in practical settings, the float ambiguity resolution is more commonly used than the best integer solution, likely due to the higher risk of significant positioning errors associated with the latter.

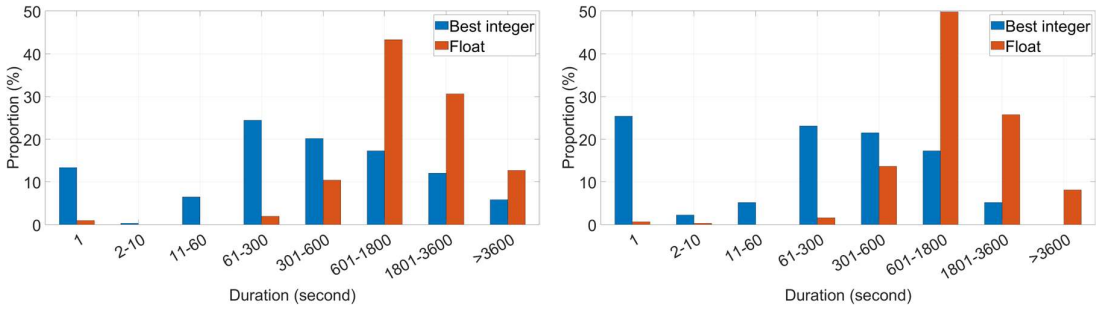

Figure 10. Convergence time with the best integer and float ambiguity resolution in vertical direction (left: dual frequency; right: multiple frequency).

4.1.3. Positioning Accuracy

This section aims to compare the positioning accuracy with correct integer ambiguity resolution if it can be fixed successfully to that with converged float ambiguity solution in the latter half hour of the hourly session.

Figures 11, 12 and 13 depict the positioning RMS in east, north and vertical directions. The benefit of correct ambiguity resolution is substantial with almost all positioning RMS much less than 5 cm in all directions. While for float ambiguity resolution, most RMS are around 5 cm and there are cases with RMS reaching several decimeters.

Preprints.org (www.preprints.org) | NOT PEER-REVIEWED | Posted: 2 July 2024 doi:10.20944/preprints202407.0220.v1

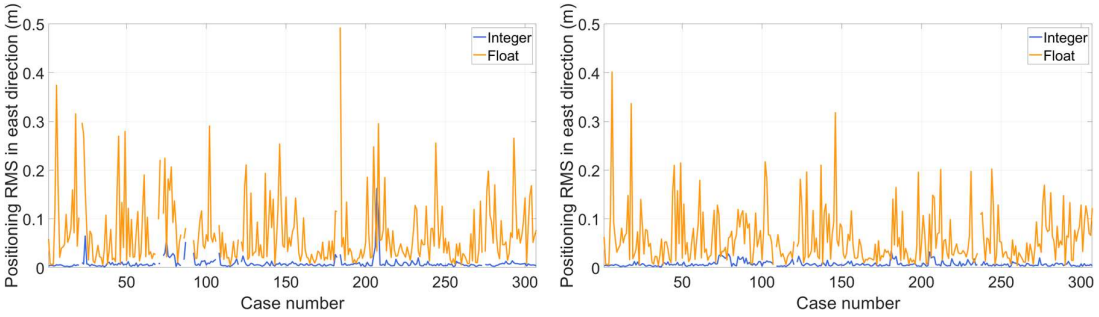

Figure 11. Positioning RMS in latter half an hour in east.

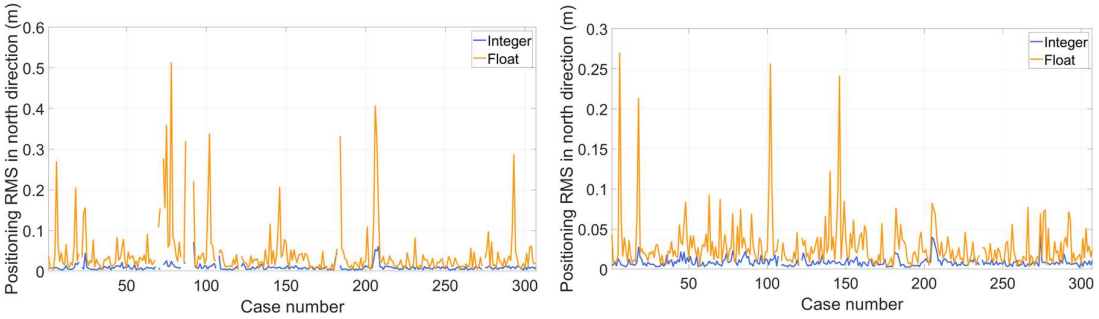

Figure 12. Positioning RMS in latter half an hour in north.

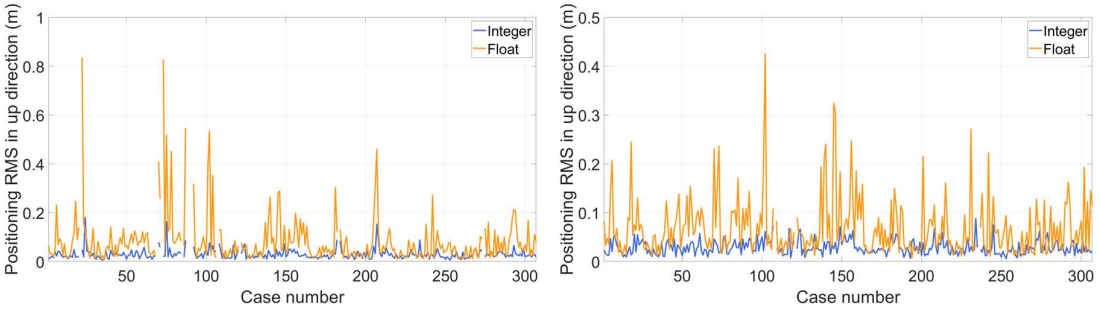

Figure 13. Positioning RMS in latter half an hour in vertical direction.

4.2. Ambiguity Validation with the Theoretical Success Rate of Ambiguity Resolution

The theoretical success rate of ambiguity resolution is often used for ambiguity validation, particularly for short-distance baseline. This study extends the investigation of its effectiveness to long-baseline scenarios. Initially, we introduce the upper and lower bounds, as well as an approximation of the success rate, following by the presentation of experimental findings.

The success rate of ambiguity resolution can be calculated according to the following formula:

$$P_s = P(\check{N} = N) = \int_{P_N} f_{\hat{N}}(x|N)dx \quad (3)$$

where, P_N is the pull-in region, $N = \{N_1, N_2, \dots, N_n\}$ is correct ambiguity, $\hat{N}$ and $\check{N}$ are float and integer ambiguity resolution respectively. $f_{\hat{N}}(x|N)$ is assumed to be the normal PDF of $\hat{N}$ with mean N and VC-matrix $Q_{\hat{N}\hat{N}}$.

Calculating the exact success rate P_s, is highly complex due to the intricate nature of P_N. Consequently, in practical scenarios, approximations or bounds are utilized instead.

The first upper bound by bounding the pull-in region is given as (Teunissen 1998a):

$$P_{Upper,1} = \prod_{i=1}^{p}(2\Phi\left(\frac{1}{2\sigma_{v_{i|I}}}\right) - 1) \quad (4)$$

 doi:10.20944/preprints202407.0220.v1

With $p < n$ and $\sigma_{v_i v_j} = \frac{u_i^T Q_{\hat{N}\hat{N}} u_j}{\|u_i\|_{Q_{\hat{N}\hat{N}}} \|u_j\|_{Q_{\hat{N}\hat{N}}}}$, u_i和$u_j \in Z^n$.

The second upper bound for Integer Least Squares (ILS) based on ADOP is given as (Hassibe and Boyd 1998; Teunissen 2000):

$$P_{Upper,2} = P\left(\chi^2(n,0) \le \frac{C_n}{ADOP^2}\right) \quad (5)$$

With $C_n = \frac{\left(\frac{2}{n}\Gamma\left(\frac{2}{n}\right)\right)^{\frac{2}{n}}}{\pi}$ and $ADOP = \sqrt{\det\left(Q_{\hat{N}\hat{N}}\right)^{\frac{1}{n}}}$.

An approximation to the ILS success rate based on ADOP can be calculated as (Teunissen 2000):

$$P_{Approximation} = \left(2\Phi\left(\frac{1}{2ADO}\right) - 1\right)^n \quad (6)$$

The first lower bound with bootstrapping (IB) can be calculated as (Teunissen 1998b):

$$P_{Lower,1} = \prod_{i=1}^{n}\left(2\Phi\left(\frac{1}{2\sigma_{\hat{N}_{i|I}}}\right) - 1\right) \quad (7)$$

where $\sigma_{\hat{N}_{i|I}}$ with $I = \{i+1, \ldots, n\}$ is the conditional variance of the i th float ambiguity $\hat{N}_i$ on the float ambiguities from $i+1$ to n.

The second lower bound with Integer Rounding (IR) based on the diagonal VC-matrix $Q_{\hat{N}\hat{N}}$ can be calculated as (Teunissen 1998b):

$$P_{Lower,2} = \prod_{i=1}^{n}\left(2\Phi\left(\frac{1}{2\sigma_{\hat{N}_i}}\right) - 1\right) \quad (8)$$

where $\sigma_{\hat{N}_i}^2$ is the diagonal element of $Q_{\hat{N}\hat{N}}$.

The third lower bound by bounding the pull-in region is given as:

$$P_{Lower,3} = P\left(\chi^2(n,0) \le \frac{1}{4}\min_{u \in Z^n \setminus \{0\}} \|u\|^2_{Q_{\hat{N}\hat{N}}}\right) \quad (9)$$

Figure 14 illustrates six different success rates over varying time durations for the experimental case involving shows these six success rates with different durations for the experimental case No. 88 (dual-frequency). The graph reveals a substantial disparity between the highest, $P_{Upper,1}$ and the lowest, $P_{Lower,3}$, with a potential difference nearing 100%. $P_{Upper,1}$ approaches 100% within a single epoch, while $P_{Upper,2}$ and $P_{Approximation}$ exhibit similar treads, both achieving approximately 99.9% within a 10 to 20-minute span. $P_{Lower,1}$ surpasses the 80% threshold after one hour, whereas $P_{Lower,2}$ does not exceed 20% even after the same duration. $P_{Lower,3}$ remains negligible, barely deviating from zero after one hour.

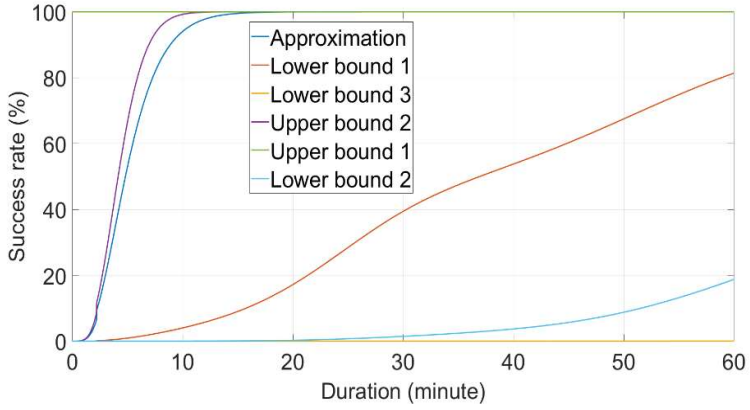

Figure 14. Success rate of experimental case No. 88 (dual frequency).

And the order of the six success rates is:

$$P_{Upper,1} > P_{Upper,2} > P_{Approximation} > P_{Lower,1} > P_{Lower,2} > P_{Lower,3}$$

The observed consistency in the order of these six success rates across all the experimental cases suggests that the exact success rate is likely to fall between $P_{Upper,2}$ and $P_{Lower,1}$ or between $P_{Approximation}$ and $P_{Lower,1}$. This observation implies that $P_{Upper,1}$, $P_{Lower,2}$ and $P_{Lower,3}$ may not be suitable for practical applications.

Preprints.org (www.preprints.org) | NOT PEER-REVIEWED | Posted: 2 July 2024 doi:10.20944/preprints202407.0220.v1

To establish the range of the exact success rate more precisely, Figure 15 displays the minimum time required for $P_{Approximation}$ to achieve a 99.999% success rate across all experimental cases, considering both dual- and multiple-frequency scenarios. Black dots indicate cases where the best integer ambiguity resolution is correct, while red dots represent incorrect resolutions. For dual-frequency cases, 50% requires less than 5 minutes to reach this level of success, and 74.3% require less than 10 minutes. In contrast, for multiple-frequency cases, 50% achieve this success rate in under half a minute, and 69.4% in under one minute. However, the prevalence of red dots indicates that the majority of cases are incorrect, 62.5% for dual-frequency and 64.2% for multiple-frequency. This suggests that $P_{Approximation}$ is likely significantly higher than the exact success rate, rendering it inapplicable as well.

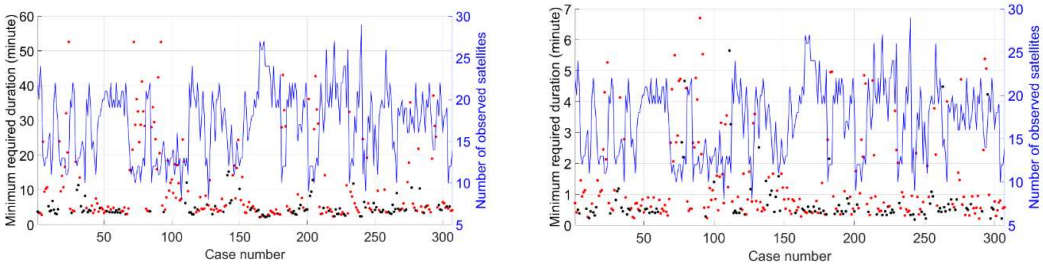

Figure 15. Minimum required time for $P_{Approximation}$ to reach 99.999% (left: dual frequency; right: multi-frequency).

Consequently, it is reasonable to infer that the exact success rate should be bracketed between $P_{Approximation}$ and $P_{Lower,1}$.

Figure 16 presents $P_{Lower,1}$ success rates for dual- and multiple-frequency cases after a one-hour duration. Black dots denote cases with correct best integer ambiguity resolution, and red dots denote incorrect resolutions. Additionally, Figure 17 provides statistics on the distribution of different $P_{Lower,1}$ values. For dual-frequency cases, 45.28% have $P_{Lower,1}$ greater than 90%, and 71.34% have $P_{Lower,1}$ greater than 80%. For multi-frequency cases, these figures are 77.20% and 89.25%, respectively. Notably, in both dual- and multi-frequency scenarios, only one case resulted in incorrect best integer ambiguity.

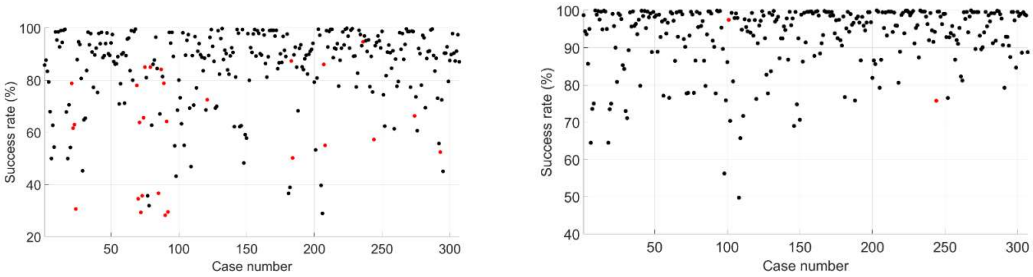

Figure 16. $P_{Lower,1}$ after one hour (left: dual frequency; right: multi-frequency).

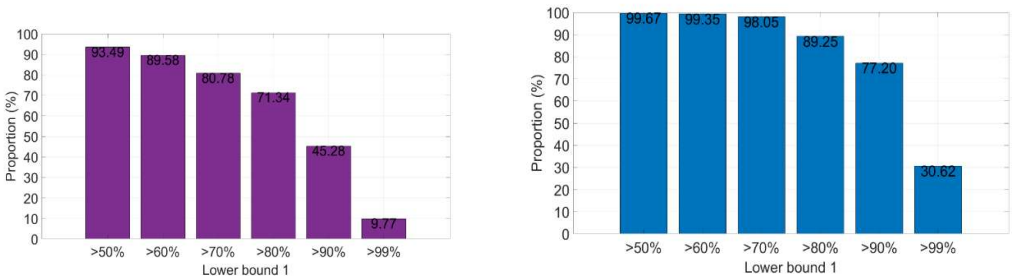

Figure 17. Statistics of $P_{Lower,1}$ after one hour (left: dual frequency; right: multi-frequency).

 doi:10.20944/preprints202407.0220.v1

Therefore, among the six evaluated success rates, $P_{Lower,1}$ appears to be the closest approximation to the exact success rate. Furthermore, Figure 17 indicates that, regardless of whether the frequency is dual or multiple, most cases can be correctly resolved within a one-hour duration.

In summary, the investigation reveals that the two upper bounds and the approximation, along with $P_{Lower,2}$ and $P_{Lower,3}$, deviate significantly from the exact success rate, being either excessively high or markedly low. Consequently, these metrics are not suitable for practical application in long-distance RTK. Although $P_{Lower,1}$ appears to be the closest to the exact success rate, its utility is limited to scenarios where long observation durations are feasible. Therefore, for practical long-distance RTK applications, reliance on $P_{Lower,1}$ may only be advisable when extended observation times are available to ensure a higher likelihood of correct ambiguity resolution.

4.3. Ambiguity Validation with R-Ratio Test

The R-ratio test is widely used in network RTK for its high reliability, typically with a threshold value of 2.0. This section delves into the R-ratio test's performance and efficacy for long-distance RTK applications.

Figures 18 and 19 display the minimum time required for the R-ratio to exceed various thresholds, 1.3, 1.4, 1.5, 1.6, 1.7, 1.8, 1.9 and 2.0, for both dual- and multi-frequency scenarios. Black dots indicate correct ambiguity resolution, while red ones signify mis-fix.

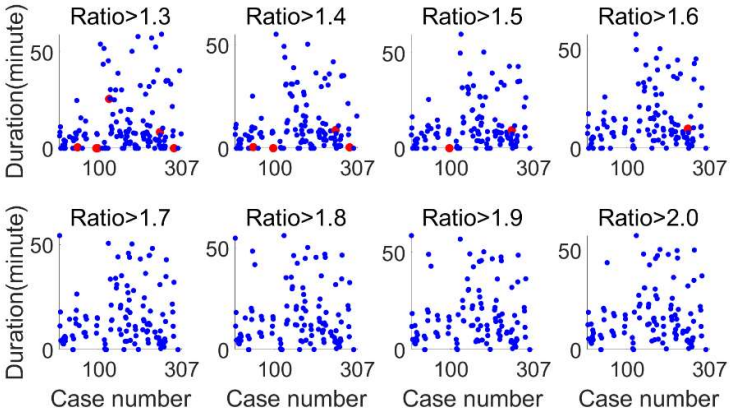

Figure 18. Minimum time required to exceed different R-ratio thresholds (dual-frequency).

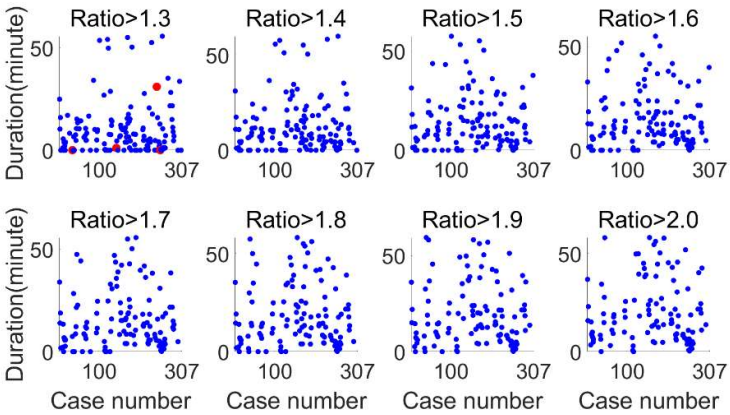

Figure 19. Minimum time required to exceed different R-ratio thresholds (multi-frequency).

In the dual-frequency scenario, mis-fixes occur at the threshold values of 1.3, 1.4, 1.5 and 1.6, with mis-fix count of 6, 4, 2 and 1, respectively. For multi-frequency, mis-fixes are observed only at a threshold value of 1.3, totaling four cases. The specifics of these mis-fixes are detailed in Table 2. It is

 doi:10.20944/preprints202407.0220.v1

observed that for dual-frequency, mis-fixed can be attributed to either a short duration, no longer than 1 minute, or a limited number of satellites, no more than 8. Similarly, for multi-frequency, one mis-fix occurred with a duration exceeding half an hour but with only 5 satellites observed, while the durations for the other three mis-fixes were 4, 4, and 69 seconds, respectively, barely over a minute.

Table 2. Detailed information of the mis-fixed experimental case.

frequency	threshold	case No.	duration (s)	satellite number
dual	1.3	46	31	14
		93	1	7
		96	2	8
		125	1539	7
		252	505	8
		287	2	12
	1.4	46	36	14
		96	3	8
		252	528	8
		287	28	12
	1.5	96	3	8
		252	567	8
	1.6	252	595	8
multiple	1.3	33	4	11
		143	69	11
		244	1860	5
		253	4	11

Table 2 presents the counts and percentages of successful ambiguity resolutions across different threshold values for dual- and multi-frequency scenarios. It is noted that, regardless of frequency, the success rate does not exceed 50% even at a threshold of 1.3, and it marginally surpasses one-third when the threshold is set to 2.0. Furthermore, the success rates for dual- and multi-frequency are quite comparable. For dual-frequency, the success rates range from 44.6% to 34.9% and for multi-frequency, from 46.3% to 35.2%.

Table 3. Statistics of success ambiguity resolution of various R-ratio threshold.

threshold	dual-frequency		multi-frequency	
	case count	proportion (%)	case count	proportion (%)
1.3	137	44.6	142	46.3
1.4	128	41.7	141	45.9
1.5	124	40.4	135	44.0
1.6	122	39.7	132	43.0
1.7	117	38.1	123	40.1
1.8	114	37.1	123	40.1
1.9	111	36.2	115	37.5
2.0	107	34.9	108	35.2

 doi:10.20944/preprints202407.0220.v1

Figures 20 and 21 provide statistical data on the time needed to achieve various R-ratio thresholds for both dual- and multi-frequency scenarios. Across all threshold values, for both dual- and multi-frequency, the most common duration to reach the threshold is within 10 minutes, followed by the 10 to 20-minute range as the second most common. When the threshold is set to 2.0, approximately 70% of dual-frequency cases and 60% of multi-frequency cases reach the threshold within 20 minutes. This suggests that if the R-ratio does not meet the threshold within 20 minutes, it is unlikely to succeed in fixing the ambiguity even with extended observation time.

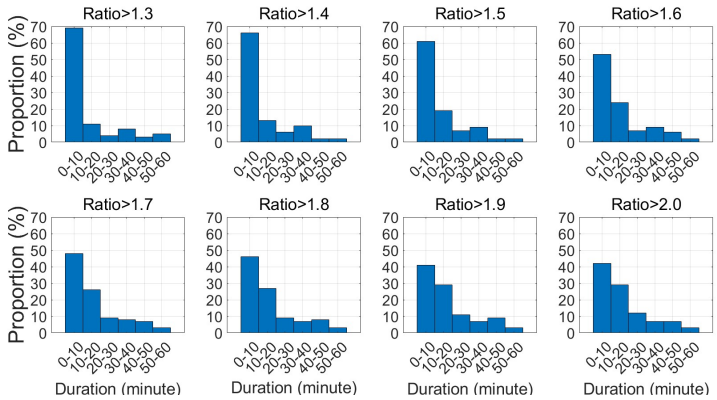

Figure 20. Duration needed to first exceed various R-ratio thresholds (dual-frequency).

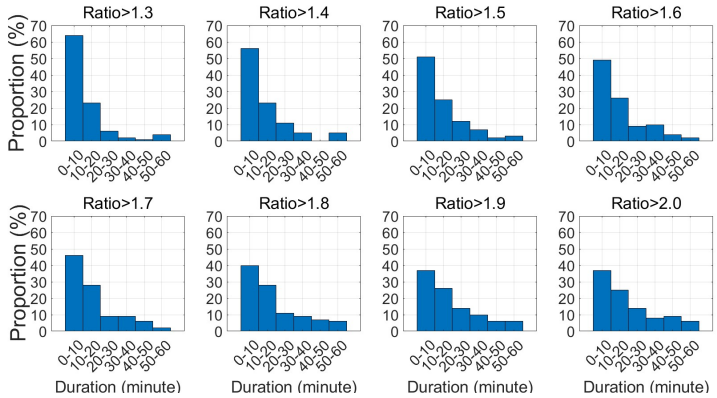

Figure 21. Duration needed to first exceed various R-ratio thresholds (multi-frequency).

To conclude, the R-ratio test tends to be more dependable for ambiguity validation when the observation duration exceeds 2 minutes and when there are more than 10 satellites being observed. A threshold value above 1.7 is recommended for better reliability. If the threshold is attainable, the required observation duration is typically no more than 20 minutes; otherwise, merely prolonging the observation time is unlikely to help the ratio meet the threshold. Additionally, the overall success rate for ambiguity resolution using the R-ratio test is relatively low, not exceeding 50% even at a threshold of 1.3, and hovering around one-third when the threshold is set to 2.0.

5. New Ambiguity Resolution Validation Method

Based on the findings, it is evident that the six theoretical success rate bounds do not align well with practical outcomes for long-distance RTK, as there is a significant discrepancy between their values and the actual ones. In the case of the R-ratio test, although it appears to be a reliable indicator with a threshold value exceeding 1.7, the likelihood of successful ambiguity resolution remains disappointingly low, dropping to merely one-third when the threshold is set at 2.0. Consequently, it appears that, for the cases unable to be fixed with the R-ratio test, resorting to float ambiguity resolution is the only viable option, which however is sometimes unreasonable.

 doi:10.20944/preprints202407.0220.v1

Illustrating this point, Figure 22 shows the experimental case No. 31 (multiple-frequency) and presents the positioning errors in the X, Y, and Z directions using both the best integer and float ambiguity resolutions, alongside the R-ratio values. The data reveals that the best ambiguity resolution is correct from onset. However, throughout the hour, the R-ratio value does not exceed 1.05. Employing the float solution may result in significantly reduced positioning accuracy compared to the integer solution, even after thirty minutes, which is both illogical and inefficient.

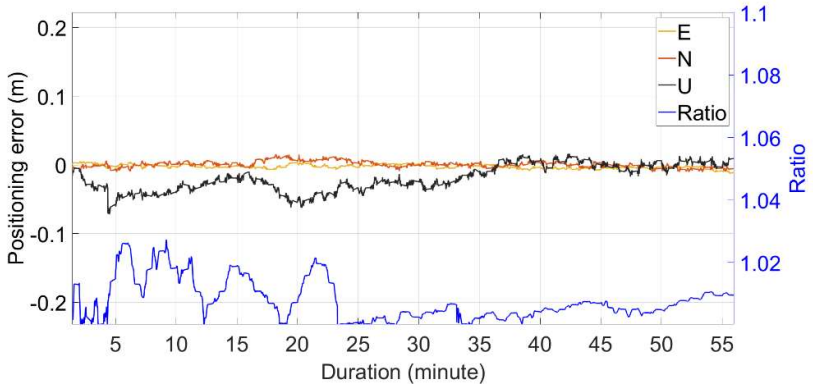

Figure 22. Positioning error with the best integer ambiguity resolution of case No. 31 (multi-frequency).

In this section, we introduce a novel method for validating ambiguity resolution that is tailored for scenarios where the R-ratio test may not be effective. Unlike conventional approaches that prioritize rapid ambiguity resolution within a few minutes or up to twenty minutes, our proposed method is designed to be applicable over more extended periods, such as thirty minutes to an hour.

Figures 23 depicts the duration for which a particular ambiguity candidate remains the best integer ambiguity resolution (indicated in blue) in comparison to the second-best candidate (shown in greed) over the course of an hour. These durations can be either continuous or intermittent. In instances where the ambiguity resolution with the longest duration is incorrect, it is marked in red. Additionally, a yellow line represents the ratio of the second-longest duration to the longest duration.

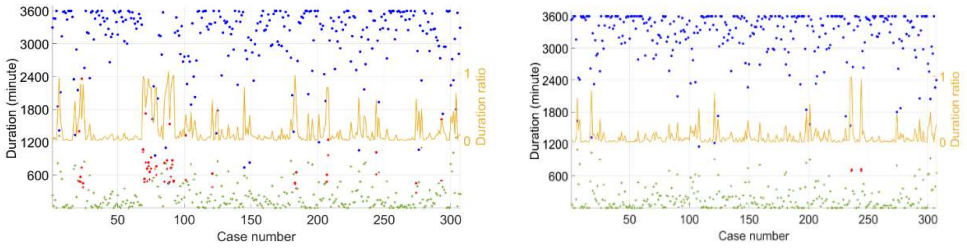

Figure 23. The longest duration vs the second longest to be the best integer ambiguity resolution (left: dual-frequency; right: multi-frequency).

Analysis of the left part reveals that for dual-frequency data, the majority of the best ambiguity resolutions with the longest durations are accurate. However, there is an 8.79% incidence of incorrect resolutions. Within this subset, there are 27 instances that exceed 10 minutes, yet all fall short of the half-hour mark, with one exception lasting 2036 seconds.

Turning to the right part, which focuses on multi-frequency data, we observe that incorrect cases are present, albeit at a lower rate of 0.65%, Among these, only two cases surpass the 10-minute threshold, and none extend beyond 1000 seconds. This suggests that the proposed method may offer a more reliable means of ambiguity validation over longer periods, particularly in multi-frequency scenarios where the duration of incorrect resolutions is notably shorter.

 doi:10.20944/preprints202407.0220.v1

6. Conclusions

In this study, which utilizes extensive data from the IGS network, a comprehensive analysis was conducted on the effectiveness of two widely adopted ambiguity validation techniques in long-distance RTK. The fundings from the numerical analysis indicate that:

- The six theoretical success rate bounds currently in use are either excessively large or small compared to the actual value, rendering them impractical for long-distance RTK applications.
- The R-ratio test proves to be generally reliable when the threshold is set above 1.7, provided that there is an adequate duration of observations (at least one minute) and a sufficient number of visible satellites (more than 10).
- The likelihood of successfully resolving ambiguities using the R-ratio test does not exceed 50%. Furthermore, if a resolution is not achieved in 20 minutes, merely extending the observation time is typically ineffective.
- In spite of different time required to exceed various R-ratio thresholds, the success rates for dual- and multi-frequency are quite comparable.

To enhance ambiguity resolution performance in practical scenarios that involve lengthy observation periods, this research introduces a new ambiguity validation approach. This method suggests that if one integer ambiguity resolution candidate maintains the best status for a significantly longer period than its runner-up, it can be confidently accepted as correct. While testing confirms the dependability of this new approach, it is notably conservative and should only be employed when the R-ratio test fails.

Consequently, the challenge of ambiguity validation in long-distance RTK remains unresolved, and there is a pressing need for innovative methods that balance reliability with efficiently.

Acknowledgment: This research was substantially supported by the National Natural Science Foundation of China (Grant Nos. 42074028, 41704021 and 41701513), the Natural Science Foundation of Shandong Province, China (Grant Nos. ZR2020MD042 and ZR2020MD065).

 doi:10.20944/preprints202407.0220.v1

Appendix A Detailed Information of Experimental Cases

Num	Case name	Receiver type	Distance (km)	GPS	Galileo	BeiDou-2	BeiDou-3	GLONASS
1	REDU-BRUX-00H	SEPT POLARX5TR SEPT POLARX5TR	104.8	L1 L2 L5	E1 E5b E5a E6 E5	B1 B2 B3	B1 B3	Y
2	REDU-BRUX-06H							
3	REDU-BRUX-12H							
4	REDU-BRUX-18H							
5	HUEG-ZIM2-00H	JAVADTRE_3L DELTA TRIMBLE NETR9	106.9	L1 L2 L5	E1 E5b E5a E5	B1 B2	B1	Y
6	HUEG-ZIM2-06H							
7	HUEG-ZIM2-12H							
8	HUEG-ZIM2-18H							
9	NANO-ALBH-00H	SEPT POLARX5 SEPT POLARX5	109.8	L1 L2 L5	E1 E5b E5a E6 E5			N
10	NANO-ALBH-06H							
11	NANO-ALBH-12H							
12	NANO-ALBH-18H							
13	NANO-UCLU-00H	SEPT POLARX5 SEPT POLARX5	113.9	L1 L2 L5	E1 E5b E5a E6 E5	B1 B2 B3	B1 B3	Y
14	NANO-UCLU-06H							
15	NANO-UCLU-12H							
16	NANO-UCLU-18H							
17	BRMG-ZIM2-00H	JAVAD TRE_3 DELTA TRIMBLE NETR9	115.3	L1 L2 L5	E1 E5b E5a E5	B1 B2	B1	Y
18	BRMG-ZIM2-06H							
19	BRMG-ZIM2-12H							
20	BRMG-ZIM2-18H							
21	USUD-CHOF-00H	SEPT POLARX5 JAVADTRE_G3TH DELTA	117.2	L1 L2 L5	E1 E5a			N
22	USUD-CHOF-06H							
23	USUD-CHOF-12H							
24	USUD-CHOF-18H							

 doi:10.20944/preprints202407.0220.v1

25	LEIJ-POTS-00H	JAVAD TRE_3 DELTA JAVAD TRE_3	123.6	L1 L2 L5	E1 E5b E5a E6 E5	B1 B2 B3	B1 B3	Y
26	LEIJ-POTS-06H							
27	LEIJ-POTS-12H							
28	LEIJ-POTS-18H							
29	BRUX-DLF1-00H	SEPT POLARX5TR TRIMBLE ALLOY	132.2	L1 L2 L5	E1 E5b E5a E5	B1 B2	B1	Y
30	BRUX-DLF1-06H							
31	BRUX-DLF1-12H							
32	BRUX-DLF1-18H							
33	BREW-DRAO-00H	SEPT POLARX5TR SEPT POLARX5	132.5	L1 L2 L5	E1 E5b E5a E6 E5			N
34	BREW-DRAO-06H							
35	BREW-DRAO-12H							
36	BREW-DRAO-18H							
37	KOS1-TIT2-00H	SEPT POLARX5E JAVAD TRE_3 DELTA	133.6	L1 L2 L5	E1 E5b E5a E6 E5	B1 B2 B3	B1 B3	Y
38	KOS1-TIT2-06H							
39	KOS1-TIT2-12H							
40	KOS1-TIT2-18H							
41	CHWK-ALBH-00H	SEPT POLARX5 SEPT POLARX5	138.2	L1 L2 L5	E1 E5b E5a E6 E5			N
42	CHWK-ALBH-06H							
43	CHWK-ALBH-12H							
44	CHWK-ALBH-18H							
45	BAUT-GOP6-00H	JAVAD TRE_3 DELTA SEPT POLARX5	143.5	L1 L2 L5	E1 E5b E5a E6 E5	B1 B2 B3	B1 B3	Y
46	BAUT-GOP6-06H							
47	BAUT-GOP6-12H							
48	BAUT-GOP6-18H							
49	BAUT-GOPE-00H	JAVAD TRE_3 DELTA TRIMBLE ALLOY	143.5	L1 L2	E1 E5b E5a E6	B1 B2 B3	B1	Y
50	BAUT-GOPE-06H							

 doi:10.20944/preprints202407.0220.v1

51	BAUT-GOPE-12H			L5	E5	B3	
52	BAUT-GOPE-18H						
53	REDU-TIT2-00H						
54	REDU-TIT2-06H	SEPT POLARX5TR		L1	E1 E5b	B1	
55	REDU-TIT2-12H	JAVAD TRE_3 DELTA	146.8	L2	E5a E6	B1 B2 B3	Y
56	REDU-TIT2-18H			L5	E5	B3	
57	BRUX-TIT2-00H						
58	BRUX-TIT2-06H	SEPT POLARX5TR		L1	E1 E5b	B1	
59	BRUX-TIT2-12H	JAVAD TRE_3 DELTA	148.1	L2	E5a E6	B1 B2 B3	Y
60	BRUX-TIT2-18H			L5	E5	B3	
61	LEIJ-BAUT-00H						
62	LEIJ-BAUT-06H	JAVAD TRE_3 DELTA		L1	E1 E5b	B1	
63	LEIJ-BAUT-12H	JAVAD TRE_3 DELTA	150.9	L2	E5a E6	B1 B2 B3	Y
64	LEIJ-BAUT-18H			L5	E5	B3	
65	NANO-CHWK-00H						
66	NANO-CHWK-06H	SEPT POLARX5		L1	E1 E5b	B1	
67	NANO-CHWK-12H	SEPT POLARX5	152.1	L2	E5a E6	B1 B2 B3	Y
68	NANO-CHWK-18H			L5	E5	B3	
69	USUD-TSK2-00H						
70	USUD-TSK2-06H	SEPT POLARX5		L1			
71	USUD-TSK2-12H	TRIMBLE ALLOY	155.4	L2	E1		N
72	USUD-TSK2-18H			L5	E5a		
73	WTZ3-GOP6-00H						
74	WTZ3-GOP6-06H	JAVAD TRE_G3TH DELTA		L1			
75	WTZ3-GOP6-12H	SEPT POLARX5	162.4	L2	E1		N
76	WTZ3-GOP6-18H			L5	E5a		

 doi:10.20944/preprints202407.0220.v1

77	WTZ3-GOPE-00H	JAVAD TRE_G3TH DELTA TRIMBLE ALLOY	162.4	L1 L2 L5	E1 E5a		N
78	WTZ3-GOPE-06H						
79	WTZ3-GOPE-12H						
80	WTZ3-GOPE-18H						
81	BAUT-POTS-00H	JAVAD TRE_3 DELTA JAVAD TRE_3	165.9	L1 L2 L5	E1 E5b E5a E6 E5	B1 B2 B3	B1 B3 Y
82	BAUT-POTS-06H						
83	BAUT-POTS-12H						
84	BAUT-POTS-18H						
85	WTZ3-OBE4-00H	JAVAD TRE_G3TH DELTA SEPT ASTERX4	166.8	L1 L2 L5	E1 E5a		N
86	WTZ3-OBE4-06H						
87	WTZ3-OBE4-12H						
88	WTZ3-OBE4-18H						
89	USUD-ISHI-00H	SEPT POLARX5 SEPT POLARX5	167.3	L1 L2 L5	E1 E5a		N
90	USUD-ISHI-06H						
91	USUD-ISHI-12H						
92	USUD-ISHI-18H						
93	CHWK-DRAO-00H	SEPT POLARX5 SEPT POLARX5	174.5	L1 L2 L5	E1 E5b E5a E6 E5		N
94	CHWK-DRAO-06H						
95	CHWK-DRAO-12H						
96	CHWK-DRAO-18H						
97	DLF1-TIT2-00H	SEPT POLARX5 SEPT POLARX5	177.0	L1 L2 L5	E1 E5b E5a E5	B1 B2	B1 Y
98	DLF1-TIT2-06H						
99	DLF1-TIT2-12H						
100	DLF1-TIT2-18H						
101	BAUT-WROC-00H	SEPT POLARX5 LEICA GR50	177.9	L1 L2	E1 E5b E5a	B1 B2	B1 Y
102	BAUT-WROC-06H						

 doi:10.20944/preprints202407.0220.v1

103	BAUT-WROC-12H			L5	E5			
104	BAUT-WROC-18H							
105	JPLM-GOLD-00H	SEPT POLARX5	179.3	L1	E1 E5b			N
106	JPLM-GOLD-06H	JAVAD TRE_G3TH DELTA		L2	E5a			
107	JPLM-GOLD-12H			L5				
108	JPLM-GOLD-18H							
109	WSRT-DLF1-00H	LEICA GR50	182.7	L1	E1 E5b	B1	B1	Y
110	WSRT-DLF1-06H	TRIMBLE ALLOY		L2	E5a	B2		
111	WSRT-DLF1-12H			L5				
112	WSRT-DLF1-18H							
113	BRUX-KOS1-00H	SEPT POLARX5TR	183.5	L1	E1 E5b	B1 B2 B3	B1	Y
114	BRUX-KOS1-06H	SEPT POLARX5TR		L2	E5a E6			
115	BRUX-KOS1-12H			L5	E5		B3	
116	BRUX-KOS1-18H							
117	FFMJ-TIT2-00H	SEPT POLARX5TR	189.9	L1	E1 E5b	B1 B2 B3	B1	Y
118	FFMJ-TIT2-06H	JAVAD TRE_3 DELTA		L2	E5a E6			
119	FFMJ-TIT2-12H			L5	E5		B3	
120	FFMJ-TIT2-18H							
121	ABMF-LMMF-00H	SEPT POLARX5	193.1	L1	E1 E5b	B1	B1	Y
122	ABMF-LMMF-06H	TRIMBLE ALLOY		L2	E5a E6			
123	ABMF-LMMF-12H			L5	E5	B3	B3	
124	ABMF-LMMF-18H							
125	NRC1-ALGO-00H	TRIMBLE ALLOY	198.6	L1	E1 E5b			N
126	NRC1-ALGO-06H	SEPT POLARX5		L2	E5a			
127	NRC1-ALGO-12H			L5				
128	NRC1-ALGO-18H							

 doi:10.20944/preprints202407.0220.v1

129	BREW-CHWK-00H	SEPT POLARX5	205.8	L1	E1 E5b	B1	B1	Y
130	BREW-CHWK-06H	SEPT POLARX5		L2	E5a E6	B2		
131	BREW-CHWK-12H			L5	E5	B3	B3	
132	BREW-CHWK-18H							
133	POTS-WARN-00H	JAVAD TRE_3	209.4	L1	E1 E5b	B1	B1	Y
134	POTS-WARN-06H	JAVAD TRE_3		L2	E5a E6	B2		
135	POTS-WARN-12H			L5	E5	B3	B3	
136	POTS-WARN-18H							
137	WSRT-TIT2-00H	JAVAD TRE_3	209.4	L1	E1 E5b	B1	B1	Y
138	WSRT-TIT2-06H	JAVAD TRE_3		L2	E5a E6	B2		
139	WSRT-TIT2-12H			L5		B3	B3	
140	WSRT-TIT2-18H							
141	WROC-GOP6-00H	JAVAD TRE_3 SEPT POLARX5	209.5	L1 L2 L5	E1 E5b E5a E5	B1 B2	B1	Y
142	WROC-GOP6-06H							
143	WROC-GOP6-12H							
144	WROC-GOP6-18H							
145	WROC-GOPE-00H	JAVAD TRE_3 TRIMBLE ALLOY	209.5	L1 L2 L5	E1 E5b E5a E5	B1 B2	B1	Y
146	WROC-GOPE-06H							
147	WROC-GOPE-12H							
148	WROC-GOPE-18H							
149	DLF1-REDU-00H	TRIMBLE ALLOY SEPT POLARX5TR	227.1	L1 L2 L5	E1 E5b E5a E5	B1 B2	B1	Y
150	DLF1-REDU-06H							
151	DLF1-REDU-12H							
152	DLF1-REDU-18H							
153	BAMF-CHWK-00H	SEPT POLARX5TR SEPT POLARX5	231.5	L1 L2	E1 E5b E5a E6	B1 B2	B1	Y
154	BAMF-CHWK-06H							

 doi:10.20944/preprints202407.0220.v1

155	BAMF-CHWK-12H			L5	E5	B3	B3	
156	BAMF-CHWK-18H							
157	LEIJ-GOP6-00H							
158	LEIJ-GOP6-06H	SEPT POLARX5TR		L1	E1 E5b	B1	B1	
159	LEIJ-GOP6-12H	SEPT POLARX5	234.0	L2	E5a E6	B2		Y
160	LEIJ-GOP6-18H			L5	E5	B3	B3	
161	LEIJ-GOPE-00H							
162	LEIJ-GOPE-06H	SEPT POLARX5TR		L1	E1 E5b	B1	B1	
163	LEIJ-GOPE-12H	TRIMBLE ALLOY	234.0	L2	E5a E6	B2		Y
164	LEIJ-GOPE-18H			L5	E5	B3	B3	
165	YARR-NNOR-00H							
166	YARR-NNOR-06H	SEPT POLARX5		L1	E1 E5b	B1	B1	
167	YARR-NNOR-12H	SEPT POLARX5TR	236.4	L2	E5a E6	B2		Y
168	YARR-NNOR-18H			L5	E5	B3	B3	
169	YAR3-NNOR-00H							
170	YAR3-NNOR-06H	SEPT POLARX5		L1	E1 E5b	B1	B1	
171	YAR3-NNOR-12H	SEPT POLARX5TR	236.5	L2	E5a E6	B2		Y
172	YAR3-NNOR-18H			L5	E5	B3	B3	
173	KOS1-REDU-00H							
174	KOS1-REDU-06H	SEPT POLARX5E		L1	E1 E5b	B1	B1	
175	KOS1-REDU-12H	SEPT POLARX5TR	246.2	L2	E5a E6	B2		Y
176	KOS1-REDU-18H			L5	E5	B3	B3	
177	LPAL-MAS1-00H							
178	LPAL-MAS1-06H	LEICA GR50		L1	E1 E5b	B1	B1	
179	LPAL-MAS1-12H	SEPT POLARX5	248.0	L2	E5a E6	B2		Y
180	LPAL-MAS1-18H			L5	E5	B3	B3	

 doi:10.20944/preprints202407.0220.v1

181	WTZ3-LEIJ-00H	JAVAD TRE_G3TH DELTA JAVAD TRE_3 DELTA	248.4	L1 L2 L5	E1 E5a			N
182	WTZ3-LEIJ-06H							
183	WTZ3-LEIJ-12H							
184	WTZ3-LEIJ-18H							
185	FFMJ-REDU-00H	JAVAD TRE_3 DELTA SEPT POLARX5TR	252.3	L1 L2 L5	E1 E5b E5a E6 E5	B1 B2 B3	B1 B3	Y
186	FFMJ-REDU-06H							
187	FFMJ-REDU-12H							
188	FFMJ-REDU-18H							
189	AJAC-GRAC-00H	LEICA GR50 LEICA GR50	252.7	L1 L2 L5	E1 E5b E5a E6 E5	B1 B2 B3	B1 B3	Y
190	AJAC-GRAC-06H							
191	AJAC-GRAC-12H							
192	AJAC-GRAC-18H							
193	AJAC-GRAS-00H	LEICA GR50 TRIMBLE NETR9	252.7	L1 L2 L5	E1 E5b E5a E5	B1 B2 B3	B1 B3	Y
194	AJAC-GRAS-06H							
195	AJAC-GRAS-12H							
196	AJAC-GRAS-18H							
197	BRMG-FFMJ-00H	JAVAD TRE_3 DELTA JAVAD TRE_3 DELTA	254.2	L1 L2 L5	E1 E5b E5a E6 E5	B1 B2 B3	B1 B3	Y
198	BRMG-FFMJ-06H							
199	BRMG-FFMJ-12H							
200	BRMG-FFMJ-18H							
201	ENAO-PDEL-00H	JAVAD TRE_3 TRIMBLE ALLOY	254.6	L1 L2 L5	E1 E5b E5a E5			N
202	ENAO-PDEL-06H							
203	ENAO-PDEL-12H							
204	ENAO-PDEL-18H							
205	WTZ3-BAUT-00H	TRIMBLE ALLOY JAVAD TRE_3 DELTA	256.2	L1 L2	E1 E5a			N
206	WTZ3-BAUT-06H							

 doi:10.20944/preprints202407.0220.v1

207	WTZ3-BAUT-12H			L5				
208	WTZ3-BAUT-18H							
209	UCLU-CHWK-00H							
210	UCLU-CHWK-06H	SEPT POLARX5	259.6	L1	E1 E5b	B1	B1	
211	UCLU-CHWK-12H	SEPT POLARX5		L2	E5a E6	B2		Y
212	UCLU-CHWK-18H			L5	E5	B3	B3	
213	STR1-SYDN-06H	SEPT POLARX5	259.9	L1	E1 E5b	B1	B1	
214	STR1-SYDN-18H	SEPT POLARX5TR		L2	E5a	B2		Y
				L5		B3	B3	
215	FFMJ-HUEG-00H							
216	FFMJ-HUEG-06H	JAVAD TRE_3 DELTA	262.9	L1	E1 E5b	B1	B1	
217	FFMJ-HUEG-12H	JAVAD TRE_3 DELTA		L2	E5a E6	B2		Y
218	FFMJ-HUEG-18H			L5	E5	B3	B3	
219	PARK-STR1-06H	SEPT POLARX5	259.9	L1	E1 E5b	B1	B1	
220	PARK-STR1-18H	SEPT POLARX5TR		L2	E5a	B2		Y
				L5		B3	B3	
221	UCLU-HOLB-00H							
222	UCLU-HOLB-06H	SEPT POLARX5	266.9	L1	E1 E5b	B1	B1	
223	UCLU-HOLB-12H	SEPT POLARX5		L2	E5a E6	B2		Y
224	UCLU-HOLB-18H			L5	E5	B3	B3	
225	ORID-SOFI-00H							
226	ORID-SOFI-06H	LEICA GR30	268.0	L1	E1 E5b	B1	B1	
227	ORID-SOFI-12H	LEICA GR30		L2	E5a E6	B2		Y
228	ORID-SOFI-18H			L5	E5	B3	B3	

 doi:10.20944/preprints202407.0220.v1

229 230	SYDN_TID1-06H SYDN_TID1-18H	SEPT POLARX5TR SEPT POLARX5	268.1	L1 L2 L5	E1 E5b E5a	B1 B2 B3	B1 B3	Y
231 232 233 234	ENAO-FLRS-00H ENAO-FLRS-06H ENAO-FLRS-12H ENAO-FLRS-18H	JAVAD TRE_3 TRIMBLE ALLOY	270.5	L1 L2 L5	E1 E5b E5a E5			N
235 236 237 238	BRMG-OBE4-00H BRMG-OBE4-06H BRMG-OBE4-12H BRMG-OBE4-18H	JAVAD TRE_3 DELTA SEPT ASTERX4	272.7	L1 L2 L5	E1 E5b E5a E6 E5	B1 B2 B3	B1 B3	Y
239 240	PARK-TID1-06H PARK-TID1-18H	SEPT POLARX5TR SEPT POLARX5	274.3	L1 L2 L5	E1 E5b E5a E6 E5	B1 B2 B3	B1 B3	Y
241 242 243 244	HLFX-UNB3-00H HLFX-UNB3-06H HLFX-UNB3-12H HLFX-UNB3-18H	SEPT POLARX5 TRIMBLE ALLOY	276.1	L1 L2 L5	E1 E5b E5a E6 E5			N
245 246 247 248	HUEG-OBE4-00H HUEG-OBE4-06H HUEG-OBE4-12H HUEG-OBE4-18H	JAVAD TRE_3L DELTA SEPT ASTERX4	276.3	L1 L2 L5	E1 E5b E5a E6 E5	B1 B2 B3	B1 B3	Y
249 250	HLFX-FRDN-00H HLFX-FRDN-06H	SEPT POLARX5 SEPT POLARX5	276.5	L1 L2	E1 E5b E5a E6			N

 doi:10.20944/preprints202407.0220.v1

251	HLFX-FRDN-12H			L5	E5			
252	HLFX-FRDN-18H							
253	WSRT-BRUX-00H							
254	WSRT-BRUX-06H	SEPT POLARX5	281.7	L1	E1 E5b	B1	B1	
255	WSRT-BRUX-12H	SEPT POLARX5TR		L2	E5a E6	B2		Y
256	WSRT-BRUX-18H			L5		B3	B3	
257	PARK_SYDN-06H	SEPT POLARX5TR	282.1	L1	E1 E5b	B1	B1	
258	PARK_SYDN-18H	SEPT POLARX5TR		L2	E5a	B2		Y
				L5		B3	B3	
259	BRUX-HERS-00H							
260	BRUX-HERS-06H	SEPT POLARX5TR	283.4	L1	E1 E5b	B1	B1	
261	BRUX-HERS-12H	SEPT POLARX5TR		L2	E5a E6	B2		Y
262	BRUX-HERS-18H			L5	E5	B3	B3	
263	BREW-ALBH-00H							
264	BREW-ALBH-06H	SEPT POLARX5TR	283.9	L1	E1 E5b			
265	BREW-ALBH-12H	SEPT POLARX5		L2	E5a E6			N
266	BREW-ALBH-18H			L5	E5			
267	MRO1-YAR3-00H							
268	MRO1-YAR3-12H	TRIMBLE NETR9	289.7	L1	E1 E5b	B1	B1	
269	MRO1-YAR3-18H	SEPT POLARX5		L2	E5a	B2		Y
				L5	E5	B3	B3	
270	MRO1-YARR-00H							
271	MRO1-YARR-06H	TRIMBLE NETR9	289.8	L1	E1 E5b	B1	B1	
272	MRO1-YARR-12H	SEPT POLARX5		L2	E5a	B2		Y
273	MRO1-YARR-18H			L5	E5	B3	B3	
274	DUND-MQZG-00H	TRIMBLE ALLOY	291.9	L1	E1 E5b	B1	B1	Y

 doi:10.20944/preprints202407.0220.v1

275	DUND-MQZG-06H	TRIMBLE ALLOY		L2	E5a E6	B2			
276	DUND-MQZG-12H			L5	E5				
277	DUND-MQZG-18H								
278	FFMJ-OBE4-00H								
279	FFMJ-OBE4-06H	JAVAD TRE_3 DELTA		L1	E1 E5b	B1	B1		
280	FFMJ-OBE4-12H	SEPT ASTERX4	293.5	L2	E5a E6	B2		Y	
281	FFMJ-OBE4-18H			L5	E5	B3	B3		
282	MQZG-OUS2-06H	TRIMBLE ALLOY		L1	E1 E5b	B1	B1	Y	
283	MQZG-OUS2-18H	SEPT POLARX5	294.5	L2	E5a E6	B2			
				L5	E5				
284	BAMF-HOLB-00H								
285	BAMF-HOLB-06H	SEPT POLARX5		L1	E1 E5b	B1	B1		
286	BAMF-HOLB-12H	SEPT POLARX5	295.0	L2	E5a E6	B2		Y	
287	BAMF-HOLB-18H			L5	E5	B3	B3		
288	BRMG-REDU-00H								
289	BRMG-REDU-06H	JAVAD TRE_3 DELTA		L1	E1 E5b	B1	B1		
290	BRMG-REDU-12H	SEPT POLARX5TR	295.6	L2	E5a E6	B2		Y	
291	BRMG-REDU-18H			L5	E5	B3	B3		
292	JOZ2-WROC-00H								
293	JOZ2-WROC-06H	TRIMBLE NETR9		L1	E1	B1			
294	JOZ2-WROC-12H	LEICA GR50	296	L2		B2	B1	Y	
295	JOZ2-WROC-18H			L5	E5				
296	LEIJ-FFMJ-00H								
297	LEIJ-FFMJ-06H	JAVAD TRE_3 DELTA		L1	E1 E5b	B1	B1		
298	LEIJ-FFMJ-12H	JAVAD TRE_3 DELTA	297.2	L2	E5a E6	B2		Y	
				L5	E5	B3	B3		

 doi:10.20944/preprints202407.0220.v1

299	LEIJ-FFMJ-18H							
300	POTS-GOP6-00H	JAVAD TRE_3 SEPT POLARX5	299.5	L1 L2 L5	E1 E5b E5a E6 E5	B1 B2 B3	B1 B3	Y
301	POTS-GOP6-06H							
302	POTS-GOP6-12H							
303	POTS-GOP6-18H							
304	POTS-GOPE-00H	JAVAD TRE_3 TRIMBLE ALLOY	299.5	L1 L2 L5	E1 E5b E5a E6 E5			Y
305	POTS-GOPE-06H							
306	POTS-GOPE-12H							
307	POTS-GOPE-18H							

 doi:10.20944/preprints202407.0220.v1

References

1. Chu F, Yang Ming (2013) GPS/Galileo long baseline computation: Method and performance analyses. GPS Solutions. 10.1007/s10291-013-0327-7.
2. Chu F, Yang M, Wu J (2016). A new approach to modernized GPS phase-only ambiguity resolution over long baselines. Journal of Geodesy. 90. 10.1007/s00190-015-0869-2.
3. Dennis O, Balwinder S, and Teunissen P (2004) Predicting the Success Rate of Long-baseline GPS+Galileo (Partial) Ambiguity Resolution, The Journal of Navigation , No. 67 (3): 385 – 401, DOI: https://doi.org/10.1017/S037346331400006X.
4. Euler H, Schaffrin B (1991) On a measure for the discernibility between different ambiguity solutions in the static-kinematic GPS-mode. In: IAG Symposia No. 107, kinematic systems in geodesy, surveying, and remote sensing. Springer, New York, pp 285–295.
5. Leick A (2004) GPS satellite surveying, 3rd ed. Wiley, New York.
6. Li B, Feng Y and Shen Y (2010a) Three carrier ambiguity resolution: Distance-independent performance demonstrated using semi-generated triple frequency GPS signals. GPS Solutions, 14(2), 177–184.
7. Li B, Feng Y, Shen Y, and Wang C (2010b) "Geometry-specified troposphere decorrelation for subcentimeter real-time kinematic solutions over long baselines." *J. Geophys. Res.* 115 (B11): 1978–2012. https://doi.org/10.1029/2010JB007549.
8. Li B, Shen Y, Feng Y, Gao W and Yang L (2014) GNSS ambiguity resolution with controllable failure rate for long baseline network RTK. Journal of Geodesy, 88(2), 99–112.
9. Li G, Geng J, Guo J, Zhou S and Lin S (2018) GPS+ Galileo tightly combined RTK positioning for medium-to-long baselines based on partial ambiguity resolution. The Journal of Global Positioning Systems, 16(1), 1–10.
10. Odolinski R, Teunissen P and Odijk D (2015) Combined GPS+ BDS for short to long baseline RTK positioning. Measurement Science and Technology, 26(4), 045801.
11. Sermet O, Salih A, Behlul N, Huseyin D, Ulkunur K, Ceren K, Nesibe G (2023) GPS + Galileo + BDS-3 medium to long-range single-baseline RTK: an alternative for network-based RTK? The Journal of Navigation, 76: 467–486 doi:10.1017/S0373463323000243.
12. Shu B, Liu H, Xu L, Qian C, Gong X and An X (2018) Performance analysis of BDS medium-long baseline RTK positioning using an empirical troposphere model. Sensors, 18(4), 1199.
13. Teunissen P (1998a) On the integer normal distribution of the GPS ambiguities. Artificial Satellites, 33(2): 49–64.
14. Teunissen P (1998b) Success probability of integer GPS ambiguity rounding and bootstrapping. Journal of Geodesy, 72: 606–612.
15. Teunissen P (2000) ADOP based upperbounds for the bootstrapped and the least-squares ambiguity success rates. Artificial Satellites, 35(4): 171–179.
16. Teunissen P, Verhagen S (2009) The GNSS ambiguity ratio-test revisited: a better way of using it. Surv Rev 41(312):138–151.
17. Xu Y, Ji S, Chen W, Weng D (2015) A New Ionosphere-free Ambiguity Resolution method for Long-range Baseline with GNSS Triple-Frequency signals. Advances in Space Research. 56. 10.1016/j.asr.2015.07.013.
18. Zhang Z, Li B and Zou J (2020a) Can long-range single-baseline RTK provide service in Shanghai comparable to network RTK? Journal of Surveying Engineering, 146(4), 05020007.
19. Zhang Y, Kubo N, Chen, J, Chu F, Wang H and Wang J (2020b) Contribution of QZSS with four satellites to multi-GNSS long baseline RTK. Journal of Spatial Science, 65(1), 41–60.